13th International Conference Series on
Laser-light and Interactions with Particles
Optical Particle Characterization follow-up !
August 21-26th, 2022, Warsaw, Poland

# HIGH THROUGHPUT LIGHT SCATTER IMAGING OF MICROPARTICLES IN FLOW CYTOMETRY

**Jonas GIENGER*, Christian GOERKE, Alexander HOPPE, Alexander PUTZ, Dirk GROSENICK, Martin HUSSELS**

Physikalisch-Technische Bundesanstalt (PTB), Abbestr. 2-12, 10587 Berlin, Germany

*Corresponding author: jonas.gienger@ptb.de*

**Abstract**

We equipped a flow cytometer with two low-cost industrial CMOS cameras to image the scattered intensity distributions of single microparticles and cells at throughputs of several hundred events per second. These images are compared to the far-field scattered intensity distributions computed with various computational methods, which yields information about particle size, shape and orientation in the fluid flow.

## 1 Introduction

In a flow cytometer, microscopic objects of interest (e. g., biological cells or artificial micro- and nanoparticles) pass through a laser focus one by one in a fluid flow. In most standard devices the scattered light is collected with detectors in the forward and sideward directions, without any angular resolution. Depending on the device, the objects flow at velocities of a few metres per second and throughput may exceed 10,000 events/s. This means that interaction times with the laser are in the microsecond range. Fluorescent labelling is often used for the differentiation of cells on a biomolecular basis.

Imaging flow cytometry combines the high information content of microscopic images with the high throughput of flow cytometry. This can be particularly useful in applications where very small populations of target cells must be identified and quantified within huge numbers of other cells, coincidences and agglomerates. Minor errors in counting those populations can have a major impact on the diagnosis. As differentiation between single cells, coincidences, and cell agglomerates is challenging for common flow cytometers, we developed a flow cytometer with integrated multi-dimensional imaging.

Our instrument combines the high signal detection rates of photomultiplier tubes (PMTs) with the ability to capture images of particles or cells of interest. Here we present data for differently shaped polystyrene and silica particles in the forward direction. Compared with light scattering simulations, this reveals the potential of the comprehensive analysis of agglomerates and coincidences by imaging for improving particle or cell counting accuracy and for label-free differentiation.

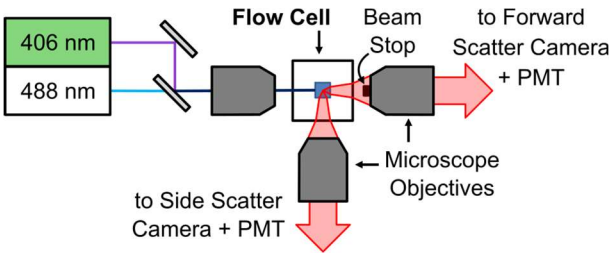


***Figure 1*** *Cytometer flow cell with lasers and objectives. The flow direction is into the image plane.*

## 2 Experiment

A schematic of the measurement setup is shown in Figure 1. We operate a continuous wave laser at 488 nm and a gated laser at 406 nm focused into the flow cell with a small offset along the flow direction. Images are captured by two low-cost industrial CMOS cameras (no side scatter images are shown in this extended abstract). Triggering of the cameras and gating of the 406 nm laser emission are controlled by an FPGA. As the same FPGA processes all data of the PMTs, this enables to set camera trigger conditions for each conventional detector channel of the setup.

When an object passes the 488 nm laser focus, the data of the PMTs is analysed by the FPGA and compared to the trigger conditions. In case all conditions are fulfilled, the cameras are triggered instantaneously, and the laser gate is shortly opened when the object will be in the focus of the 406 nm laser. This results in a short laser flash (0.1 µs to

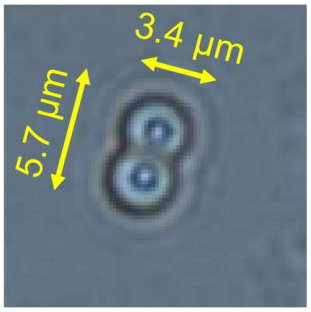


***Figure 2*** *Microscope image of a hybrid silica "dumbbell" particle.*

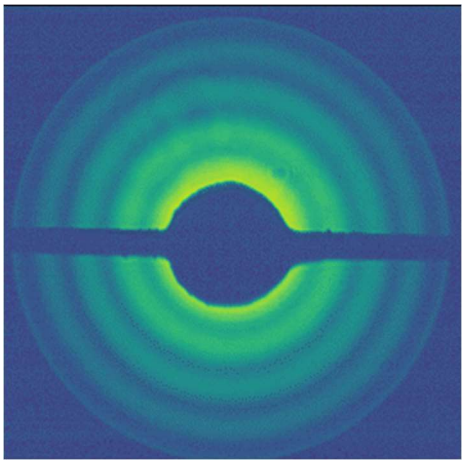

***Figure 3*** *Measured forward scatter image of a single hybrid silica sphere (presumably 3.4μm diameter) in water at 406nm wavelength. Logarithmic intensity scale.*

1 μs) on the object being much shorter than the minimum exposure time (>59 μs) of the cameras to prevent motion blur. This way, we can benefit from low-cost industrial cameras to capture sharp images at high flow velocities (~2 m/s). Currently, we can set a trigger window for each PMT detector channel, but more complex trigger conditions are possible.

## 3 Simulations

To aid the interpretation of the scattered light intensity distributions, we perform light scattering simulations for different classes of particle shapes. Lorenz-Mie Theory (LMT) can be used for single spherical particles. For coincidences of two (or more) spherical particles passing the laser simultaneously, we use the T-matrix method, specifically the multiple sphere T-matrix (MSTM) code [1]. For general aspherical particles we use the discrete dipole approximation (DDA) framework and employ the ADDA code [2].

Using the amplitude scattering matrices or Mueller matrices from these numerical simulations we can compute far-field intensity distributions $I(\theta, \phi)$ over the angles in the medium inside the flow cell (here water) for a given laser polarization (along the flow direction). The images in the experiment are recorded with a microscope objective and subsequent additional optics outside of the flow cell and surrounded by air (see Figure 1). To compare the simulated patterns with measured ones, we need to take into account the refraction of light rays at the interfaces of the flow cell (water-quartz and quartz-air) to find the mapping $\rho = g(\theta)$ from angles inside to flow cell to positions in the forward principal plane of the microscope objective. For the forward scatter direction this would be $\rho = z \tan\theta$ with $z = f$ (focal length of the objective) in the absence of interfaces. With two plane-parallel interfaces, a relation $\rho = g(\theta)$ can be found based on Snell's law and basic geometry. To display

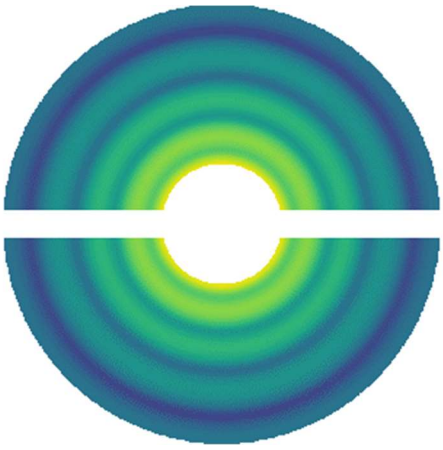

***Figure*** *4 Simulated forward scatter image for a single hybrid silica sphere.*

the simulated intensity pattern like the measured images, this mapping needs to be applied and the far-field intensity values $I(\theta, \phi)$ then need to be scaled according to the element of area of the mapping $g$ according to conservation of energy/power. This accounts for oblique incidence and yields

$$\tilde{I}(\rho, \phi) = I(\theta, \phi) \frac{\sin(\theta)}{g(\theta)} \frac{1}{g'(\theta)}. \quad (1)$$

The inverse relation can be used to extract far-field intensity distributions $I(\theta, \phi)$ from the measured images $\tilde{I}(\rho, \phi)$.

## 4 Particles and Simulation Parameters

We show here results for particles made from a hybrid silica material with an estimated refractive index of 1.41 at 406nm. Figure 2 shows a microscope image of a "dumbbell" shaped particle (microparticles GmbH, Berlin. Germany) which consists of two fused spheres. For light scattering simulations these particles are modelled using the bi-sphere model in ADDA with a centre-to-centre distance smaller than the sphere diameter ($R_{cc}/d \approx 0.6$) to have the spheres overlapping in the centre of the particle and match the size of 5.7μm by 3.4μm as specified by the manufacturer.

The spot size of the laser in the cytometer is sufficiently large compared to the particle size (>10μm along the narrow direction) such that we assume plane-wave illumination in all the simulations. The surrounding medium is pure water with an RI of 1.343 [3].

## 5 Results

Even though the particle suspension was manufactured to contain dumbbell-shaped particles, it also contains a significant percentage of single spheres. The measured scattering pattern from such a spherical particle is shown in Figure 3, which can be compared to the simulation result in Figure 4. Logarithmic intensity scales are used in all images shown here. In the measurements, the direct laser beam is blocked before the microscope objective (see Figure 1) to avoid over-exposure of the camera. The beamstop has the

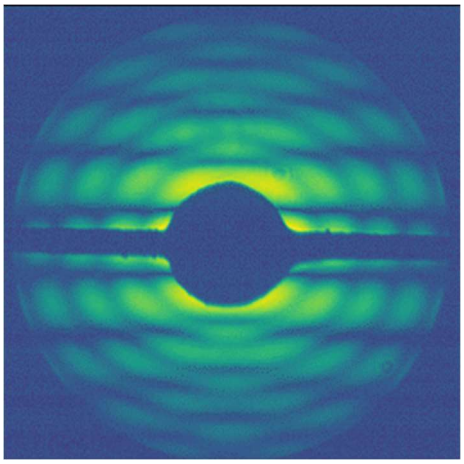

***Figure 5*** *Measured forward scatter image of a single hybrid silica dumbbell (3.4µm wide, 5.7µm long).*

shape of a circular disc on a strip (for mounting) and can be clearly seen as a dark region in the measurements. This area was also removed in the simulated images. Figures 5 and 6 show measurement and simulation results for a dumbbell particle oriented along the flow direction (vertical axis in the images). In addition to the spherical pattern from a single sphere, horizontal stripes are visible, that correspond to the length of the particle.

## 6 Conclusion

Our setup can capture images of the intensity distribution of the light scattered by single microparticles in flow at a high throughput. These can be compared to numerical simulations from various light-scattering frameworks for different particles. In this presentation we discuss how these data can be used to obtain information about the individual particles. For example, for spherical particles, fitting the parameters of the LMT (diameter and refractive index) can allow for accurate particle characterization. For non-spherical particles or coincidences/aggregates of spheres, the scattered intensity pattern carries information about shape and orientation in flow. Combining imaging in the forward and side directions is particularly useful in this case. The measurements can readily be extended to biological cells. This could, for example yield information about their deformation in flow or simply to distinguish coincidences. However, finding accurate simulation models might be more challenging for these more complex biological objects than for artificial particles.

## 7 References

[1] Mackowski D.W., Mishchenko M.I., A multiple sphere T-matrix Fortran code for use on parallel computer clusters, Journal of Quantitative Spectroscopy and Radiative Transfer, 112(13):2182–92 (2011)

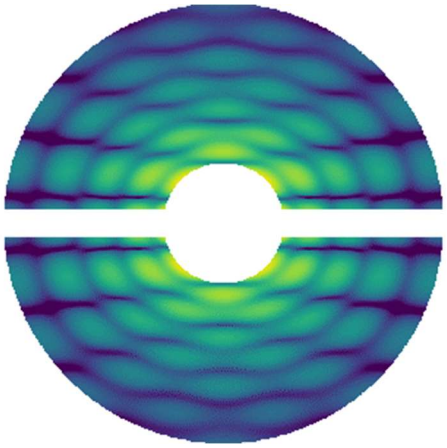

***Figure 6*** *Simulated forward scatter image for a single hybrid silica dumbbell.*

[2] Yurkin M.A., Hoekstra A.G., The discrete-dipole-approximation code ADDA: Capabilities and known limitations, Journal of Quantitative Spectroscopy and Radiative Transfer, 112(13):2234–47 (2011)

[3] Daimon M., Masumura A., Measurement of the refractive index of distilled water from the near-infrared region to the ultraviolet region, Applied Optics 46(18):3811–20 (2007)